


Article

Facile Synthesis and Environmental Applications of Noble Metal-Based Catalytic Membrane Reactors

Haochen Yan ¹, Fuqiang Liu ¹, Jinna Zhang ^{2,*} and Yanbiao Liu ^{1,3,*} 

¹ College of Environmental Science and Engineering, Textile Pollution Controlling Engineering Center of the Ministry of Ecology and Environment, Donghua University, Shanghai 201620, China

² State Key Laboratory of Urban Water Resource and Environment, School of Environment, Harbin Institute of Technology, Harbin 150090, China

³ Shanghai Institute of Pollution Control and Ecological Security, Shanghai 200092, China

* Correspondence: jnzhang@hit.edu.cn (J.Z.); yanbiaoliu@dhu.edu.cn (Y.L.); Tel.: +86-21-6779-8752 (Y.L.)

Abstract: Noble metal nanoparticle-loaded catalytic membrane reactors (CMRs) have emerged as a promising method for water decontamination. In this study, we proposed a convenient and green strategy to prepare gold nanoparticle (Au NPs)-loaded CMRs. First, the redox-active substrate membrane (CNT-MoS₂) composed of carbon nanotube (CNT) and molybdenum disulfide (MoS₂) was prepared by an impregnation method. Water-diluted Au(III) precursor (HAuCl₄) was then spontaneously adsorbed on the CNT-MoS₂ membrane only through filtration and reduced into Au(0) nanoparticles in situ, which involved a “adsorption–reduction” process between Au(III) and MoS₂. The constructed CNT-MoS₂@Au membrane demonstrated excellent catalytic activity and stability, where a complete 4-nitrophenol transformation can be obtained within a hydraulic residence time of <3.0 s. In addition, thanks to the electroactivity of CNT networks, the as-designed CMR could also be applied to the electrocatalytic reduction of bromate (>90%) at an applied voltage of −1 V. More importantly, by changing the precursors, one could further obtain the other noble metal-based CMR (e.g., CNT-MoS₂@Pd) with superior (electro)catalytic activity. This study provided new insights for the rational design of high-performance CMRs toward various environmental applications.

Keywords: catalytic membrane reactor; noble metal catalyst; carbon nanotubes; molybdenum disulfide; water purification



Citation: Yan, H.; Liu, F.; Zhang, J.; Liu, Y. Facile Synthesis and Environmental Applications of Noble Metal-Based Catalytic Membrane Reactors. *Catalysts* **2022**, *12*, 861. <https://doi.org/10.3390/catal12080861>

Academic Editor: Hideyuki Katsumata

Received: 7 July 2022

Accepted: 3 August 2022

Published: 5 August 2022

Publisher's Note: MDPI stays neutral with regard to jurisdictional claims in published maps and institutional affiliations.



Copyright: © 2022 by the authors. Licensee MDPI, Basel, Switzerland. This article is an open access article distributed under the terms and conditions of the Creative Commons Attribution (CC BY) license (<https://creativecommons.org/licenses/by/4.0/>).

1. Introduction

Recently, catalytic membrane reactors (CMRs) have attracted considerable attention for various environmental applications [1–3]. In a typical CMR, catalysts could be attached on or embedded in varying substrate materials [4]. This strategy allows the catalytic reaction and separation process to occur simultaneously in a single operational unit without the necessity for a catalyst post-separation [5,6]. In comparison to conventional batch systems, such a flow-through design features enhanced mass transport by convection, operability, and scalability. However, it is still a grand challenge to rationally design a high-performance CMR with excellent catalytic reactivity and separation efficiency.

Gold nanoparticles (Au NPs) have been regarded as promising catalysts due to their excellent catalytic performance, which have been applied in many important industrial sectors, such as CO oxidation, hydrogenation reaction, and alcohols oxidation [7–9]. The specific properties of Au NPs are highly dependent on their nanoscale size and high surface area [10]. Although these nanoparticles exhibit a better catalytic performance, the direct use of these nano-catalysts can hardly be achieved due to particle aggregations and the post-separation of catalyst from solution [11–13]. These restrictions significantly increase the cost, thus hindering wide industrial applications. To overcome these limitations, significant efforts have been devoted to constructing catalytic membrane reactors (CMRs) by integrating the noble metal nanocatalysts with supporting materials [14,15]. Researchers

have developed various strategies to immobilize these nanoparticles onto carriers, including coprecipitation, impregnation, and/or in situ growth [16]. However, these typical methods usually involve toxic hazardous reducing and/or stabilizing chemical reagents [17–19]. In addition, the harsh flow conditions during catalysis may wash out these catalysts from the host surface, which would ultimately lead to an evident performance decay over continuous running cycles. It is, therefore, highly desirable to develop rapid, robust, and environmentally-friendly CMRs preparation protocols.

Alternatively, the emerging two-dimensional transition metal dichalcogenides, molybdenum disulfide (MoS_2), may have the potential to address the mentioned problems due to their advantages of low toxic and sulfur-rich properties [20,21]. Studies have demonstrated that MoS_2 , with abundant active sulfur sites, have a high affinity for special metal ions (e.g., Pb(II) , Ag(I) and Au(III)) via Lewis soft–soft interactions [22–24]. On the other hand, it has been found that the adsorbed noble metal ions onto MoS_2 can spontaneously capture the electrons released by Mo(IV) to achieve their synchronous reduction, avoiding the need for additional reductants (e.g., NaBH_4) [25–27]. For example, our recently work showed that the MoS_2 nanoflowers could achieve the effective recovery of gold from complex wastewater involving a two-step adsorption–reduction process [28–30].

Furthermore, the substrate membrane used in the CMR also plays a unique role to construct a robust system. Various substrates with high stability and water flux have been reported, such as alumina, polymeric, and graphene oxide [31–33]. Among these support materials, one-dimensional carbon nanotubes (CNT) may be considered an ideal substrate due to its porosity, high mechanical strength, large specific surface area, rich surface chemistry, and electroactivity [34–37]. Moreover, CNT can easily be assembled into 3D porous and conductive networks by the vacuum filtration route. Therefore, this easy-modification material could provide a promising platform for improving the stability and dispersion of MoS_2 .

In this study, we adopted a rapid and green approach to synthesize the Au-immobilized CMR (CNT- MoS_2 @Au). The MoS_2 -modified CNT (CNT- MoS_2) membrane was fabricated by a simple one-step impregnation method. The MoS_2 nanoflowers on the membrane surface allowed the adsorption of $[\text{AuCl}_4]^-$ and the in situ reduction of the adsorbed anions to Au NPs free of spiking any reducing agents. Morphological, compositional, and structural characterization were performed to collectively verify the successful synthesis of Au NPs on the CNT- MoS_2 -supporting membrane. The catalytic performance of the as-prepared CNT- MoS_2 @Au membrane was evaluated using the hydrogenation of 4-nitrophenol (4-NP) as a model reaction, owing to its well-established characterization protocol and operational simplicity. The effects of key operational parameters on the performance of membrane reactors were systematically investigated. The electrocatalytic reduction of bromate (BrO_3^-) was also employed as another model reaction to demonstrate the excellent electrocatalytic characteristics of the CNT- MoS_2 @Au membrane. Finally, the non-specificity of CNT- MoS_2 membrane for loading different noble metals was emphasized by regulating the precursors.

2. Results and Discussion

2.1. Facile Synthesis of CNT- MoS_2 @Au Catalytic Membrane

Figure 1 illustrated a facile strategy for the construction of a CNT- MoS_2 @Au catalytic membrane. The MoS_2 was prepared through a hydrothermal process and the CNT membrane was synthesized via a vacuum filtration route [38]. By impregnating the CNT membrane in 15 mL of well-dispersed MoS_2 ethanol solution (1 mg/mL) for 90 min, the CNT- MoS_2 membrane was obtained after a further heat treatment (140 °C for 1 h). To endow catalytic activity for the CNT- MoS_2 membrane, Au NPs were loaded onto the membrane by passing through the noble metal salt solution (20 mL of 0.1 mM HAuCl_4) at a flow rate of 3 mL/min and pH 4.8 for 90 min. Consequently, a CNT- MoS_2 @Au catalytic membrane reactor was constructed. Notably, when compared to conventional synthesis routes, the filtration approach takes less time to achieve the uniform introduction of Au NPs (e.g., 90 min vs. 48 h) [39]. As filtration proceeded, the color of the Au(III) solution

visibly changed from light yellow to colorless, whereas the color of the membrane changed from black to brown-gold (Figure S1), suggesting that Au had been successfully deposited onto the surface of the CNT-MoS₂ membrane. A CNT-alone membrane was prepared as a control. After passing through 20 mL of 0.1 mM HAuCl₄ for 90 min, no visible color change occurred, demonstrating that a negligible Au(III) was retained by the CNT-only membrane. This observation also highlighted the essential role played by MoS₂ for anchoring Au(III).

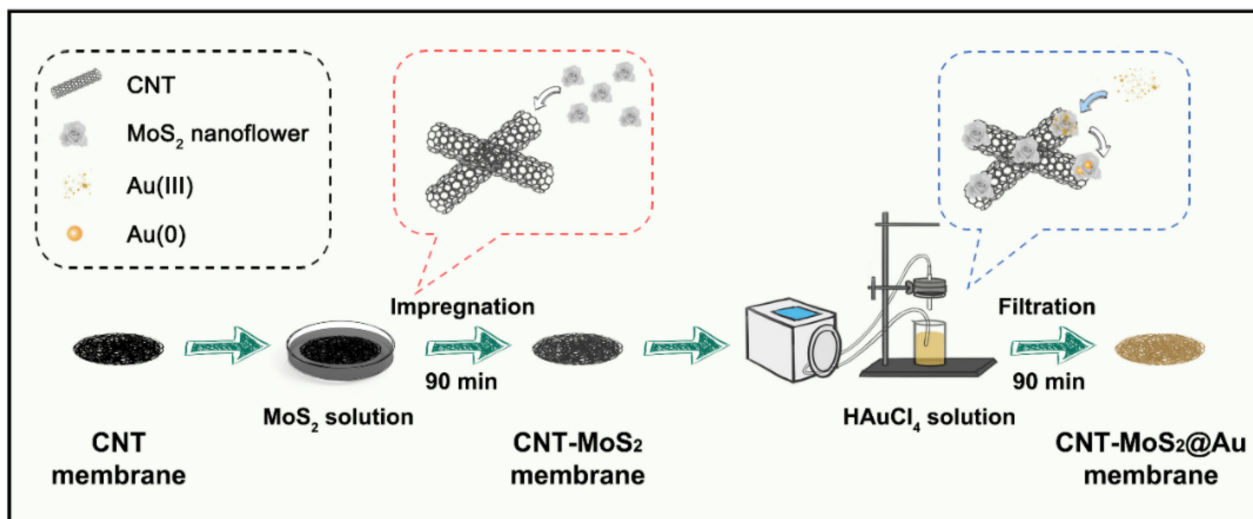


Figure 1. Schematic illustration for the synthesis of the CNT-MoS₂@Au catalytic membrane.

2.2. Characterization of the CNT-MoS₂@Au Catalytic Membrane

Figure 2a showed the FESEM image of the CNT-MoS₂@Au membrane. Typically, MoS₂ presented as nanoflowers composed of ultrathin lamellar structures with an average diameter of 400 nm (Figure S2) [38]. Numerous spherical nanoparticles were observed after the Au loading, while those MoS₂ nanoflowers were disappeared. Similar observations were reported previously [38]. These bright spherical nanoparticles were later proven to be metallic Au by using XPS and XRD characterization. The disappearance of the MoS₂ nanoflowers may be attributed to the high relative atomic mass of Au, leading to a collapse of the MoS₂ nanoflower structure during the operation. We used FESEM to monitor the evolution of the catalytic membrane surface during the Au loading process. Figure S3a showed that MoS₂ retained the nanoflower-like structure during the first 30 min and those Au NPs were observed to deposit on the edge of MoS₂ lamellar structures. The energy dispersive spectroscopy (EDS) was applied to illustrate the elemental distribution for Mo, S and Au (Figure S3b). The high-degree morphological consistence among these elements confirmed the successful loading of Au onto MoS₂ (Figures S2, S3a and 2a). The XPS spectra showed that the superficial elemental atomic ratio of the CNT-MoS₂@Au membrane was 67.83% C, 8.21% O, 4.74% S, 0.06% Mo, and 19.17% Au (Figure S4). Among them, the high-resolution Au 4f scan over a small energy window indicated two sets of Au 4f spin–orbit coupling doublets was observed (Figure 2b), with the 4f_{5/2} and 4f_{7/2} centered at 87.6 and 83.9 eV, which were associated with characteristic of Au(0) [40], suggesting an adsorption–reduction of Au(III) occurred on the membrane’s surface. XRD analysis also indicated that four distinct diffraction peaks corresponding to metallic Au(0) located at a 2θ of 38.2° (111), 44.6° (200), 64.7° (220), and 77.6° (311) were identified (Figure S5) [41].

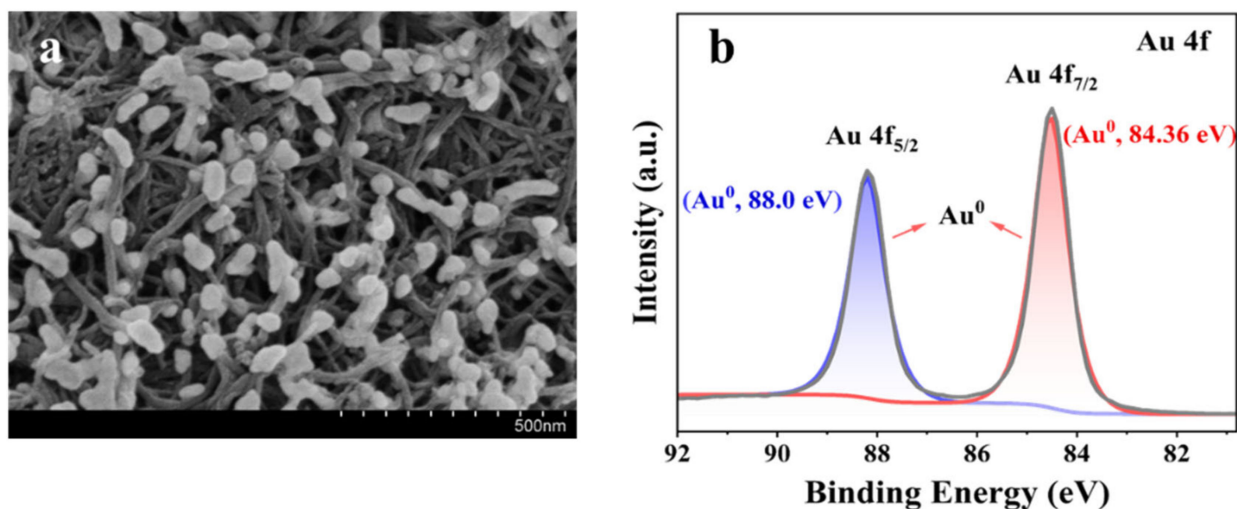


Figure 2. Preparation and characterization of the CNT-MoS₂@Au catalytic membrane. (a) FESEM image and (b) high resolution Au 4f XPS spectrum of CNT-MoS₂@Au.

2.3. Hydrogenation Reaction of 4-NP

The hydrogenation reaction of 4-NP was employed as a model catalytic reaction to compare the catalytic performance before and after the Au loading. In a control experiment, the characteristic peak of 4-NP ($\lambda_{\max} = 400$ nm) occurred no distinctive change after the solution (0.1 mM 4-NP and 30 mM NaBH₄) passed through the CNT-MoS₂ membrane (Figure S6). This indicated that the unfunctionalized CNT-MoS₂ membrane made no effort toward the 4-NP reduction. In comparison, the 4-NP characteristic absorption peak quickly decreased once the mixture solution passing through the CNT-MoS₂@Au and CNT-MoS₂@Pd membrane. The simultaneous appearance of an alternative absorption peak at 300 nm corresponded to the presence of 4-aminophenol (4-AP). This confirmed that over 95% of 4-NP was reduced by an effective hydrogenation process just after a single-pass through the catalytic membrane in the presence of NaBH₄. Notably, the ultrahigh catalytic activity of the membrane was demonstrated by an extremely short hydraulic retention time of <2 s [42]. Since the NaBH₄ concentration significantly exceeds that of 4-NP, the reaction kinetics can be considered as pseudo-first-order (Equation (1)) [43].

$$\ln(C_t/C_0) = -kt \quad (1)$$

To optimize the catalytic performance, the effects of Au(III) loading time, flow rate, and initial 4-NP concentration on the reduction of 4-NP were investigated. First, the effect of loading time of Au(III) (30, 60, 90, and 120 min) on the catalytic performance of CNT-MoS₂@Au membrane was explored, since the loading time was directly correlated to the introduced Au catalysts. CNT-MoS₂@Au membranes were characterized by XPS to investigate the alternation of Au loading time. The XPS survey pattern at different loading times (30 and 90 min) suggested that the atomic ratio of Au increased with the loading time (Figure S4). Results indicated that increasing the loading time from 30 to 90 min led to an improvement in the reduction efficiency of 4-NP (0.1 mM) from 69.6% to 92.5% at 2 mL/min under pH 8.0 (Figure 3a). This phenomenon can be ascribed to the better accessibility of 4-NP with Au NPs at an increased Au loading. However, the catalytic efficiency failed to increase significantly once the loading time further extended to 120 min (92.6%), which may be associated with the agglomeration of Au NPs (Figure S7) and burying certain available active sites with a longer loading times. Therefore, the loading time was fixed at 90 min for the subsequent investigations.

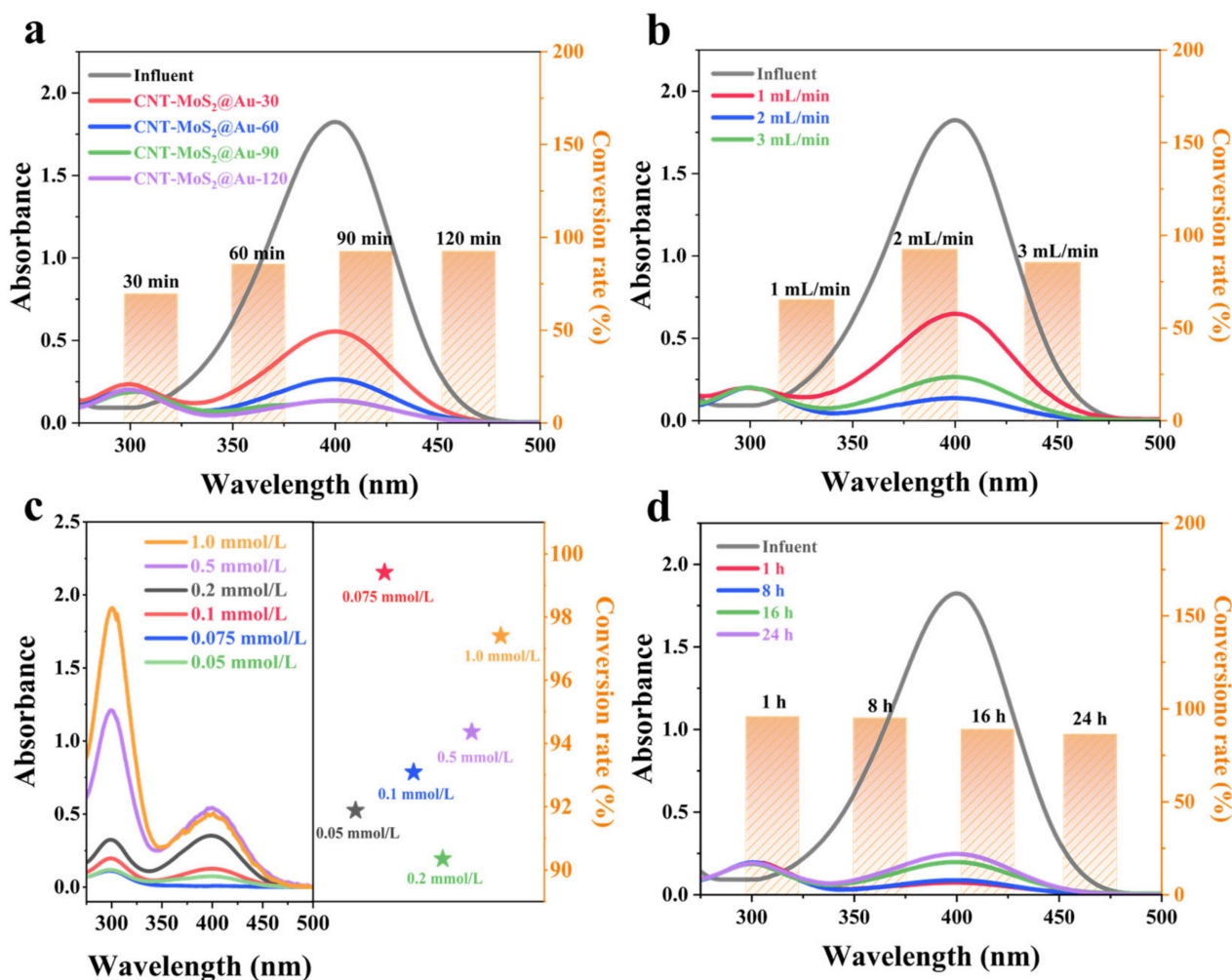


Figure 3. Effects of (a) Au loading time (30 to 120 min), (b) flow rate (1 to 3 mL/min), and (c) initial 4-NP concentration (0.05 to 1.0 mM) on the conversion of 4-NP using the CNT-MoS₂@Au catalytic membrane. (d) Operating stability in the 4-NP reduction using the CNT-MoS₂@Au catalytic membrane (24 h).

The catalytic performance of CNT-MoS₂@Au membrane was also affected by the flow rate. As shown in Figure 3b, increasing the flow rate from 1.0 to 2.0 mL/min significantly enhanced the reduction efficiency of 4-NP (0.1 mM) from 65.4% to 92.5% at pH 8.0. Nevertheless, the further increase of the flow rate to 3.0 mL/min would lead to an incomplete conversion of 4-NP (85.3%). This could be derived from the emergence of a “trade-off” effect between the 4-NP residence time within the CNT-MoS₂@Au membrane and the reaction kinetics. A lower flow rate might result in a limited mass transport within the flow-through system, whereas an excessive flow rate would bring short residence time for 4-NP and thus caused inadequate contact with the Au NPs [14].

Figure 3c showed the influence of the initial 4-NP concentration on the catalytic reduction of 4-NP. Results indicated that the CNT-MoS₂@Au membrane could effectively reduce 4-NP (>90%), regardless of the initial concentrations (from 0.05 to 1.0 mM). This suggested that the catalytic membrane had an excellent resistance to varying concentrations of 4-NP, possibly due to the effective loading of Au NPs, which provides abundant active sites for the transformation of 4-NP.

The turnover frequency (TOF), which indicates the products that are able to be generated in a catalytic reaction by the per molar amount of catalyst, was employed to quan-

tatively evaluate the catalytic performance. The TOF of the CNT-MoS₂@Au membrane under flow catalysis was calculated by Equation (2):

$$\text{TOF} = C_0 \times \text{Conversion} \times v / N_{Au} \quad (2)$$

where C_0 is the initial concentration of 4-NP (mol), N_{Au} is the molarity of Au in CNT-MoS₂@Au membrane (mol), and v is the flow rate (mL/min). Table S1 showed that the TOF value of CNT-MoS₂@Au CMR reached 609 h⁻¹ with a flow rate of 2 mL/min, which represented a much better catalytic performance than some reported reaction systems.

To further gain insight into the operating stability of the CNT-MoS₂@Au catalytic membrane, we performed a long-time (24 h) catalytic reduction experiment for 4-NP (0.1 mM) transformation in the single-pass mode at a flow rate of 2 mL/min under pH 8.0. Results exhibited that the conversion efficiency of 4-NP could maintain >86% after the continuous operation (Figure 3d). Importantly, high catalytic activity (~95%) could be recovered just by washing the membrane with copious water for a few minutes. In addition, the catalytic performance (e.g., 95.2% after 480 min) for 4-NP was comparable or even better than that of other reported CMR, such as the β -lactoglobulin fibrils membrane (>97% after 240 min) [14] and microporous polymer monoliths (~90% after ~40 min) [44]. This suggested a promising potential application of the CNT-MoS₂@Au membrane to create CMR for industrial applications.

2.4. Electrocatalytic Reduction of BrO₃⁻

Because of the excellent electrochemical properties of the CNT networks, the CNT-MoS₂@Au membrane was presumed to have excellent electrocatalytic capacity. To confirm this speculation, the electrochemical reduction of BrO₃⁻ was performed without dosing additional reducing agents. First, the control experiment was conducted to explore the electroreduction of BrO₃⁻ (0.1 mM) by the CNT-MoS₂ membrane at a flow rate of 2 mL/min under pH 4.0 (Figure S8). Negligible change in BrO₃⁻ concentration was observed and no Br⁻ was detected within 90 min regardless of the exertion of an electric field or not. This result revealed that the CNT-MoS₂ membrane was unable to electrochemically reduce BrO₃⁻ in the absence of Au NPs. For the CNT-MoS₂@Au membrane at 0 V, the result was similar with that of CNT-MoS₂ membrane. However, effective BrO₃⁻ reduction (90.1%) was achieved when a potential of -1.0 V was exerted on the CNT-MoS₂@Au membrane. The IC spectra exhibited a quick decrease of the BrO₃⁻ accompanied with the formation of Br⁻ during the electrocatalytic treatment (Figure 4c). As displayed in the inset chart, the total concentration of BrO₃⁻ and Br⁻ was slightly less than the initial total BrO₃⁻ concentration, which could be attributed to the formation of byproducts. This positive result demonstrated that the as-prepared CNT-MoS₂@Au membrane possess good electrocatalytic activity under electric field.

To obtain optimal electrocatalytic performance, the effect of applied potential on BrO₃⁻ reduction was explored. As shown in Figure 4b, all obtained data fitted the pseudo-first-order kinetic model well ($R^2 > 0.9$). Decreasing the potential from 0 to -1 V substantially improved the BrO₃⁻ reduction efficiency from ~0 to 90.1%. Nevertheless, further decreasing the potential to -2 V significantly inhibited the reduction of BrO₃⁻ (58.4%), which could be ascribed to the BrO₃⁻ reduction being highly potential-dependent and the occurrence of other side reactions (e.g., hydrogen evolution reaction). Applying a proper electric field (e.g., -1 V) to the CNT-MoS₂@Au membrane could significantly enhance near-surface transport by electromigration [45]. Meanwhile, electrostatic interactions between the negatively-charged BrO₃⁻ and positively-charged membrane surface was beneficial to the electrocatalytic reaction. However, other competitive side reactions, such as hydrogen evolution or electro-corrosion, would deteriorate the catalytic performance when the applied potential exceeded the optimal value [46–48].

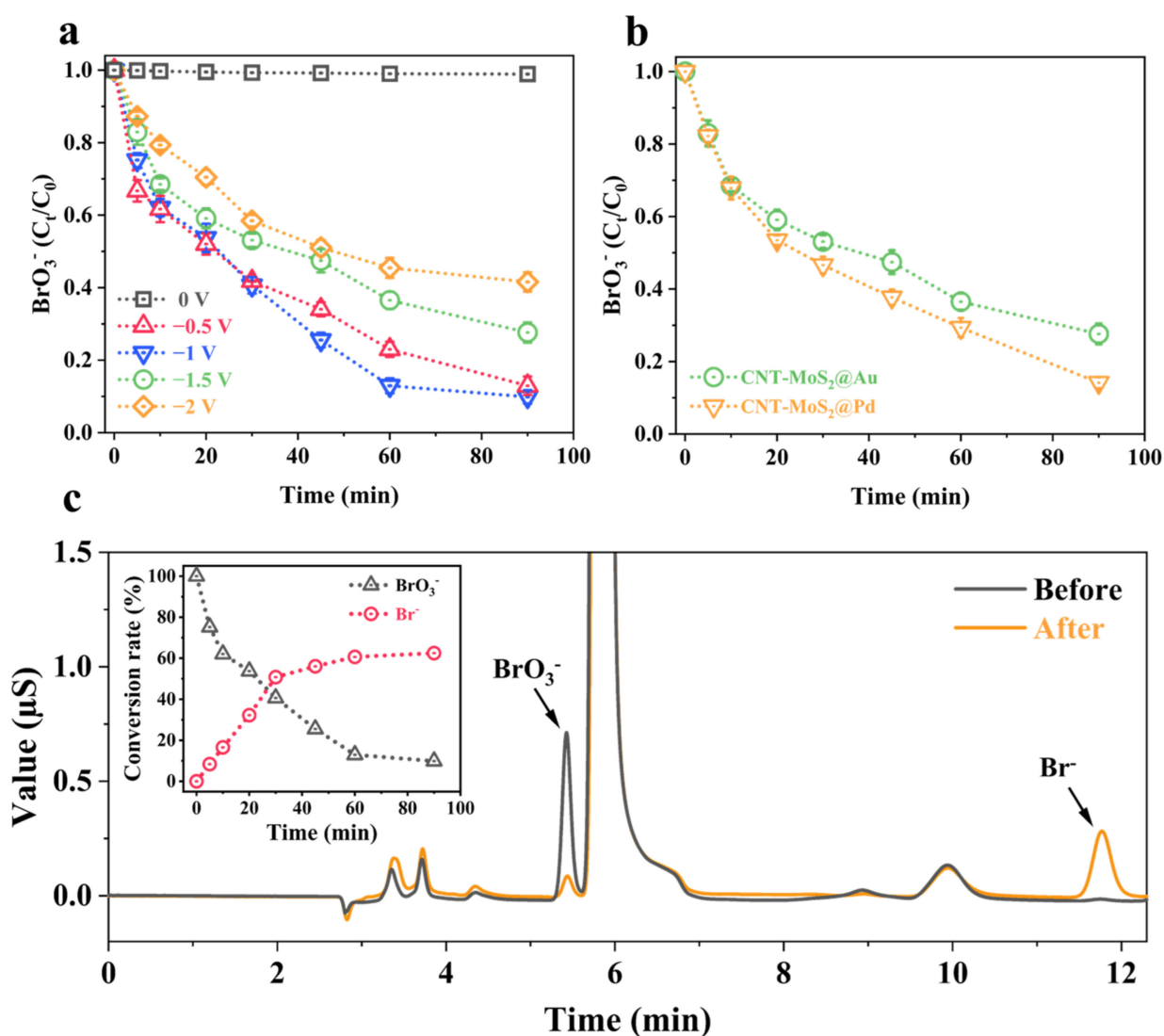


Figure 4. (a) Effect of applied potential (0 to -1.5 V) on BrO_3^- reduction using the CNT-MoS₂@Au catalytic membrane. (b) Comparison of effects on BrO_3^- reduction using different catalytic membrane. (c) IC spectra of the BrO_3^- solution before and after the electrocatalytic treatment. Inset is a comparison of the conversion efficiency towards BrO_3^- and Br^- within 90 min.

To better understand the different electrocatalytic activity of the CNT-MoS₂ membrane before and after Au NPs loading, CV and EIS measurements were carried out to determine the changes in electrochemical properties. As shown in Figure 5a, the redox peaks and current response of CNT-MoS₂@Au were higher and sharper than that of CNT-MoS₂. These results confirmed that CNT-MoS₂@Au exhibited better electrochemical activity and more rapid electron transfer process. In addition, it has been reported that the potential difference (ΔE_p) between the oxidation peak and reduction peak is inversely correlated to the charge transfer kinetics. The ΔE_p of the CNT-MoS₂@Au was 0.72-fold higher than that of CNT-MoS₂ (0.206 V vs. 0.279 V), demonstrating the charge transfer rate of CNT-MoS₂@Au was 1.37-fold than that of CNT-MoS₂ [49,50]. The EIS spectra also showed that the charge transfer resistance of CNT-MoS₂@Au (24.5 Ω) was similar with that of CNT-MoS₂ (32.5 Ω) (Figure 5b) and consistent with the CV results. This evidence suggested that the loading of Au NPs onto the CNT-MoS₂ membrane can improve the electrochemical capacitance and electron transfer kinetics, thus providing an ideal platform toward the electrocatalytic reduction of BrO_3^- .

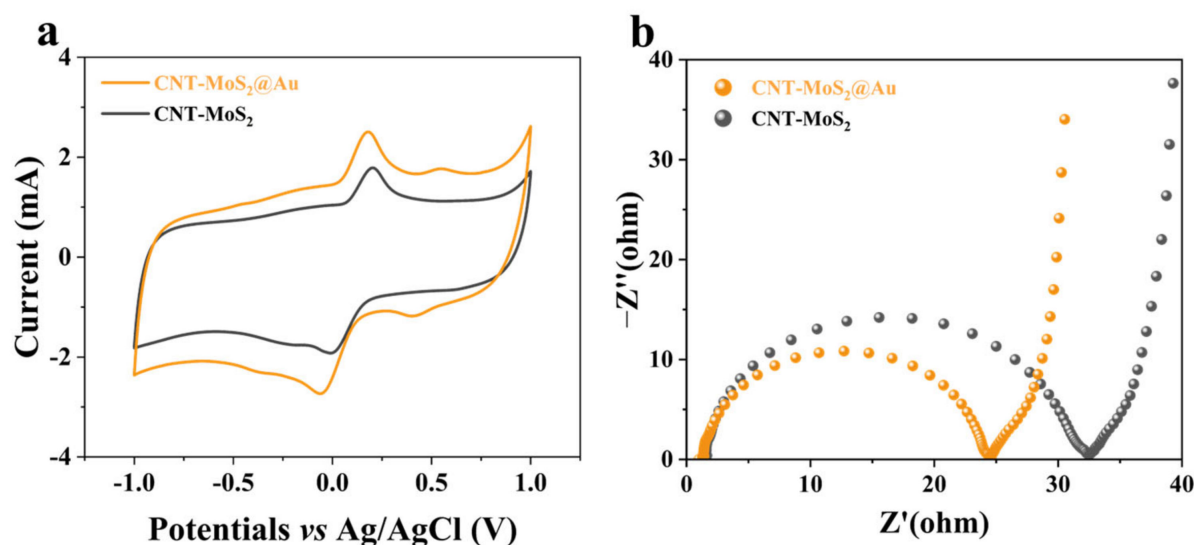


Figure 5. (a) CV and (b) EIS spectra of the CNT-MoS₂ membrane and CNT-MoS₂@Au catalytic membrane. The electrolyte contains 50 mM Na₂SO₄ and 5 mM K₃[Fe(CN)₆]. The CV scan rate was 5 mV/s. The amplitude and scan range in EIS were 5 mV and 10⁵–10^{−2} Hz, respectively.

2.5. Generality of the Electrocatalytic Membranes

According to our previous report, besides Au, MoS₂ also exhibited a high affinity towards other noble metals (e.g., Pd). Following the similar synthesis routes, we prepared a CNT-MoS₂@Pd membrane by using different Pd-based precursors to replace HAuCl₄. As displayed in Figure 4b, the designed Pd-loaded catalytic membranes also demonstrated excellent performance (85.8%) toward the electrocatalytic reduction of BrO₃[−] under similar reaction conditions (loading 90 min, flow rate = 2 mL/min, pH = 4, applied potential = −1.5 V). According to previous reports, most reported synthesis protocols for Pd-loaded catalysts usually involve complicated processes or time-consuming steps, such as microemulsion and calcination [51,52]. It is of note that our adopted approach is highly desirable (e.g., short fabrication time and comparable or even higher catalytic activity). It not only recovers noble metal ions from water but can also directly serve as high-performance (electro)catalytic membranes for environmental applications. In other words, our proposed method can be applied to prepare multiple noble metal-loaded CMRs.

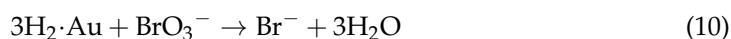
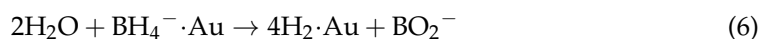
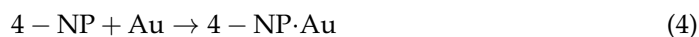
2.6. Working Mechanism of the Au-Immobilized CMR

Based on the previous discussion, it was inferred that a redox reaction occurred between Au(III) and MoS₂ following Equation (3). Au(III) was first adsorbed onto the surface of MoS₂ nanoflowers under an action of chemical chelation between Au and S, then Au(III) was able to achieve an in situ reduction to metallic AuNPs through capture the electron transfer released by the Mo(IV) [38]. This demonstrated that by impregnating the CNT-MoS₂ membrane with the Au(III) precursor (i.e., HAuCl₄), the Au NPs were successfully immobilized on the membrane through the adsorption–reduction process. Similarly, this simple protocol was adaptable to the loading of other noble metal catalysts.



For the 4-NP hydrogenation reaction, 4-NP molecules were firstly attached to the surface of Au NPs together with NaBH₄. NaBH₄ then transferred electrons to Au to generate molecular hydrogen, which contributed to the reduction of the nitro group of 4-NP to amino group. Finally, the generated 4-AP diffused away from the catalysts surface to free up the active catalytic sites for further reduction process [53]. Detailed steps involved are described by Equation (4) to Equation (8). Similar processes occurred in the electrochemical reduction as well. In the electrocatalytic system, molecular hydrogen was dissociated

in the process of water electrolysis and adsorbed into the Au NPs forming Au hydride (Au NPs also served as the cathode) [54]. These Au hydrides participated in the removal of oxygen atoms from bromate by hydrogenation [46]. This process can be expressed by Equations (9) and (10). Overall, the immobilized Au NPs offered excellent catalytic capability in the heterogeneous catalytic system.



3. Materials and Methods

3.1. Chemicals and Materials

All chemicals were of analytical grade and used without further purification. Multi-walled carbon nanotubes were provided by TimesNano Co., Ltd. (Chengdu, China). N-methyl-2-pyrrolidinone (NMP, $\geq 99.5\%$), ethanol ($\text{C}_2\text{H}_5\text{OH}$, $\geq 96\%$), thiourea ($\text{CH}_4\text{N}_2\text{S}$, $\geq 99\%$), sodium molybdate ($\text{Na}_2\text{MoO}_4 \cdot 2\text{H}_2\text{O}$, $\geq 99\%$), hydrochloric acid (HCl, 36.0~38.0%), sodium bromate (NaBrO_3 , $\geq 99\%$), sodium sulfate (Na_2SO_4 , $\geq 99\%$), potassium ferricyanide ($\text{K}_3[\text{Fe}(\text{CN})_6]$, $\geq 99\%$), palladium chloride (PdCl_2 , $\geq 99\%$), and sodium borohydride (NaBH_4 , $\geq 98\%$) were obtained from Sinopharm Chemical Reagent Co., Ltd. (Beijing, China). Au(III) chloride trihydrate ($\text{HAuCl}_4 \cdot 3\text{H}_2\text{O}$, $\geq 49\%$) and 4-nitrophenol (4-NP, $\geq 99\%$) were provided by Sigma-Aldrich (St. Louis, MO, USA). Ultrapure water produced from a Milli-Q Direct 8 purification system (Millipore, Burlington, MA, USA) was used for all experiments.

3.2. Fabrication of Catalytic Membrane Reactors

The CNT-MoS₂ membrane was fabricated according to a reported protocol [38]. The CNT-MoS₂@Au catalytic membrane was prepared by a simple filtration route with an effective membrane area of 7.1 cm² (Figure S9). In brief, the HAuCl_4 solution (20 mL, 1 mM) was continuously passed through the CNT-MoS₂ membrane and then returned at a flow rate of 3.0 mL/min. The Au loading on the CNT-MoS₂ membrane can be adjusted by changing the filtration time (30 to 120 min). To demonstrate the non-specificity of the CNT-MoS₂ membrane, the CNT-MoS₂@Pd catalytic membrane was also prepared by a similar procedure with PdCl_2 solution as precursor (20 mL, 1 mM). All propulsion was provided by a peristaltic pump (Ismatec ISM833C, Glattbruch-Zurich, Switzerland).

3.3. Catalytic Filtration Experiments

All catalytic filtration experiments were performed on a operated in a Whatman polycarbonate filtration casing (Whatman, Dassel, Germany) [36]. The hydrogenation of 4-NP was applied to evaluate the catalytic performance of the CNT-MoS₂@Au membrane. Initially, to eliminate the effect of the physical adsorption on the 4-NP removal, 100 mL of 0.1 mM 4-NP solution was first passed through the CNT-MoS₂@Au membrane to achieve adsorption saturation at 2.0 mL/min. The hydrogenation reaction was induced by passing through the membrane with 0.1 mM 4-NP solution together with 30 mM freshly prepared NaBH_4 at pH 8.0. The effects of Au(III) loading time (30 to 120 min), flow rate (1 to 3 mL/min), and initial 4-NP concentration (0.05 to 1.0 mM) on the catalytic performance were investigated systematically. The flow rate was controlled by a peristaltic pump and the solution pH was adjusted by 1 M NaOH and/or HCl. Effluent samples were collected at specific time intervals and characterized by a UV-vis spectrophotometer.

To demonstrate the excellent electrocatalytic reactivity of the CNT-MoS₂@Au membrane, the electrocatalytic reduction of bromate (BrO₃[−]) was employed as another model reaction in a Whatman polycarbonate filtration casing with electrochemistry modifications (Figure S10) [55]. Applied potential was controlled by a CHI 660E electrochemical workstation (Chenhua Co., Ltd., Shanghai, China) in a typical three-electrode system with a CNT-MoS₂@Au working electrode, a saturated Ag/AgCl reference electrode and a Ti sheet counter electrode. In a typical electrocatalytic experiment, 20 mL of 0.1 mM NaBrO₃ solution with 4 mM Na₂SO₄ were passed through the membrane at 2.0 mL/min and pH 4.0 in the recirculated filtration mode. The impact of applied potential (−2 to 0 V) on the BrO₃[−] reduction kinetics was optimized. Furthermore, the electrocatalytic reduction experiment was conducted by applying the CNT-MoS₂@Pd membrane to similar conditions. Effluent samples were collected with a 2 mL centrifuge tube and immediately filtered through a 0.22-μm cellulose acetate membrane. The concentration of BrO₃[−] was determined by ion chromatography (IC). The conversion efficiency (%) was obtained by Equation (11):

$$\text{Conversion efficiency (\%)} = 100 \times (C_0 - C) / C_0 \quad (11)$$

where C_0 and C are the substrate concentration before or after passing through the noble metal-loaded CNT-MoS₂ membrane.

3.4. Characterization

The morphology of the CNT-MoS₂@Au membranes were characterized by field emission scanning electron microscopy (FESEM, S-4800, Hitachi, Tokyo, Japan) and energy dispersive spectroscopy (EDS, JEM-2100F). X-ray diffraction (XRD) patterns of the samples were acquired by a Rigaku D/max-2550/PC X-ray diffractometer (Rigaku, Tokyo, Japan) with Au radiation within the range of 5 to 90°. X-ray photoelectron spectroscopy (XPS) was conducted at a Thermo Fisher Scientific Escalab 250Xi (Waltham, MA, USA) under high vacuum. The concentrations of 4-NP were determined by an UV-2600 Shimadzu ultraviolet–visible spectrophotometry (Shimadzu, Kyoto, Japan) at λ_{max} of 400 nm. The concentrations of BrO₃[−] were determined by Thermo Scientific Dionex Aquion IC using an IonPac AS11-HC column and 20 mM KOH eluent. The electrochemical activity of the catalytic membranes was probed by cyclic voltammetry (CV) and electrochemical impedance spectroscopy (EIS). Cyclic Voltammetry (CV) was acquired at a scan rate of 5 mV/s in a three-electrode system. EIS analysis was performed over a frequency range of 10⁵ to 10^{−2} Hz at an amplitude of 5 mV.

4. Conclusions

In summary, we have successfully developed a facile and green approach to prepare varying noble metal-based CMRs for water purification. The as-synthesized redox-active CNT-MoS₂ membrane served as a robust platform, which enabled a rapid uptake of various noble metal (e.g., Au(III) and Pd(II)) precursors only by passing through the porous and conductive networks. The in situ adsorption–reduction of noble metal ions can be achieved spontaneously. In addition, the constructed CNT-MoS₂@Au membrane reactors demonstrated excellent (electro)catalytic activity and thus achieved the effective reduction of 4-NP (>99%) and bromate (>90%) within a hydraulic residence time of <2 s, which was comparable to or even better than several state-of-the-art reports. Overall, this study would significantly improve the sustainability and cost-effectiveness of (electro)catalytic reduction technologies toward water decontamination.

Supplementary Materials: The following supporting information can be downloaded at: <https://www.mdpi.com/article/10.3390/catal12080861/s1>. Figure S1: Electronic photos of (a) the CNT-MoS₂ membrane and (b) the CNT-MoS₂@Au membrane; Figure S2: FESEM image of CNT-MoS₂ membrane; Figure S3: (a) FESEM and (b) FESEM-EDS mapping images of CNT-MoS₂@Au-30 membrane (Au loading time, 30 min); Figure S4: Comparison of the XPS survey spectrums of CNT-MoS₂@Au catalytic membrane with different Au loading time (30 and 90 min); Figure S5: The XRD pattern of the

CNT-MoS₂@Au catalytic membrane; Figure S6: Degradation efficiency of 4-NP by using CNT-MoS₂ membrane, CNT-MoS₂@Au membrane and CNT-MoS₂@Pd membrane. Experimental conditions: [4-NP]₀ = 0.1 mM, flow rate = 2.0 mL/min and pH₀ = 8.0; Figure S7: FESEM image of CNT-MoS₂@Au-120 membrane (Au loading time, 120 min); Figure S8: Degradation efficiency of bromate by using CNT-MoS₂ membrane and CNT-MoS₂@Au membrane before and after applying potential. Experimental conditions: [BrO₃⁻]₀ = 0.1 mM, flow rate = 2.0 mL/min and pH₀ = 4.0; Figure S9: Schematic illustration of the flow-through electrocatalytic filtration system; Figure S10: Schematic diagram of electrochemistry-modified Whatman polycarbonate filtration casing; Table S1: Comparison of the 4-NP reduction performance of proposed system with reported catalytic membrane reactor systems; Table S2: The k values related to bromate reduction under different applied potential according to pseudo-first order kinetic model. References [56–60] are cited in the Supplementary Materials.

Author Contributions: Conceptualization, Y.L.; Data curation, H.Y. and F.L.; Funding acquisition, J.Z.; Investigation, H.Y. and F.L.; Methodology, H.Y. and F.L.; Project administration, Y.L. and J.Z.; Resources, Y.L.; Supervision, Y.L. and J.Z.; Writing—original draft, H.Y. and F.L.; Writing—review and editing, Y.L. and J.Z. All authors have read and agreed to the published version of the manuscript.

Funding: This work was supported by the National Natural Science Foundation of China (No. 52070055) and Heilongjiang Touyan Innovation Team Program (HIT-SE-01).

Data Availability Statement: All data supporting this study are available in the Supplementary Information accompanying this paper.

Conflicts of Interest: The authors declare no conflict of interest.

References

1. Sun, M.; Wang, X.; Winter, L.R.; Zhao, Y.; Ma, W.; Hedtke, T.; Kim, J.-H.; Elimelech, M. Electrified membranes for water treatment applications. *ACS EST Eng.* **2021**, *1*, 725–752. [[CrossRef](#)]
2. Liu, Y.; Liu, X.; Yang, S.; Li, F.; Shen, C.; Huang, M.; Li, J.; Nasaruddin, R.R.; Xie, J. Rational design of high-performance continuous-flow microreactors based on gold nanoclusters and graphene for catalysis. *ACS Sustain. Chem. Eng.* **2018**, *6*, 15425–15433. [[CrossRef](#)]
3. Peng, F.; Xu, J.; Xu, H.; Bao, H. Electrostatic interaction-controlled formation of pickering emulsion for continuous flow catalysis. *ACS Appl. Mater. Interfaces* **2021**, *13*, 1872–1882. [[CrossRef](#)]
4. Zeng, Z.; Wen, M.; Yu, B.; Ye, G.; Huo, X.; Lu, Y.; Chen, J. Polydopamine induced in-situ formation of metallic nanoparticles in confined microchannels of porous membrane as flexible catalytic reactor. *ACS Appl. Mater. Interfaces* **2018**, *10*, 14735–14743. [[CrossRef](#)] [[PubMed](#)]
5. Dolatkah, A.; Jani, P.; Wilson, L.D. Redox-responsive polymer template as an advanced multifunctional catalyst support for silver nanoparticles. *Langmuir* **2018**, *34*, 10560–10568. [[CrossRef](#)]
6. Yu, Y.; Huo, H.; Zhang, Q.; Chen, Y.; Wang, S.; Liu, X.; Chen, C.; Min, D. Nano silver decorating three-dimensional porous wood used as a catalyst for enhancing azo dyes hydrogenation in wastewater. *Ind. Crops Prod.* **2022**, *175*, 114268. [[CrossRef](#)]
7. Jia, Z.; Ben Amar, M.; Yang, D.; Brinza, O.; Kanaev, A.; Duten, X.; Vega-González, A. Plasma catalysis application of gold nanoparticles for acetaldehyde decomposition. *Chem. Eng. J.* **2018**, *347*, 913–922. [[CrossRef](#)]
8. Li, Y.; Lan, J.Y.; Liu, J.; Yu, J.; Luo, Z.; Wang, W.; Sun, L. Synthesis of gold nanoparticles on rice husk silica for catalysis applications. *Ind. Eng. Chem. Res.* **2015**, *54*, 5656–5663. [[CrossRef](#)]
9. Chen, J.; Yan, D.; Xu, Z.; Chen, X.; Chen, X.; Xu, W.; Jia, H.; Chen, J. A novel redox precipitation to synthesize Au-doped α -MnO₂ with high dispersion toward low-temperature oxidation of formaldehyde. *Environ. Sci. Technol.* **2018**, *52*, 4728–4737. [[CrossRef](#)]
10. Mistry, H.; Reske, R.; Zeng, Z.; Zhao, Z.-J.; Greeley, J.; Strasser, P.; Cuenya, B.R. Exceptional size-dependent activity enhancement in the electroreduction of CO₂ over Au nanoparticles. *J. Am. Chem. Soc.* **2014**, *136*, 16473–16476. [[CrossRef](#)]
11. Smirnov, E.; Peljo, P.; Scanlon, M.D.; Girault, H.H. Interfacial redox catalysis on gold nanofilms at soft interfaces. *ACS Nano* **2015**, *9*, 6565–6575. [[CrossRef](#)]
12. Kim, S.H. Nanoporous gold: Preparation and applications to catalysis and sensors. *Curr. Appl. Phys.* **2018**, *18*, 810–818. [[CrossRef](#)]
13. Priece, P.; Adekunle Salami, H.; Padilla, R.H.; Zhong, Z.; Lopez-Sanchez, J.A. Anisotropic gold nanoparticles: Preparation and applications in catalysis. *Chin. J. Catal.* **2016**, *37*, 1619–1650. [[CrossRef](#)]
14. Huang, R.; Zhu, H.; Su, R.; Qi, W.; He, Z. Catalytic membrane reactor immobilized with alloy nanoparticle-loaded protein fibrils for continuous reduction of 4-nitrophenol. *Environ. Sci. Technol.* **2016**, *50*, 11263–11273. [[CrossRef](#)]
15. Tong, J.; Matsumura, Y.; Suda, H.; Haraya, K. Experimental study of steam reforming of methane in a thin (6 μ M) Pd-based membrane reactor. *Ind. Eng. Chem. Res.* **2005**, *44*, 1454–1465. [[CrossRef](#)]
16. Nieto-Sandoval, J.; Gomez-Herrero, E.; Munoz, M.; de Pedro, Z.M.; Casas, J.A. Palladium-based catalytic membrane reactor for the continuous flow hydrodechlorination of chlorinated micropollutants. *Appl. Catal. B* **2021**, *293*, 120235. [[CrossRef](#)]

17. Narayanan, K.B.; Park, H.H.; Han, S.S. Synthesis and characterization of biomatrixed-gold nanoparticles by the mushroom *flammulina velutipes* and its heterogeneous catalytic potential. *Chemosphere* **2015**, *141*, 169–175. [[CrossRef](#)]
18. Tian, F.; Zhou, J.; Fu, R.; Cui, Y.; Zhao, Q.; Jiao, B.; He, Y. Multicolor colorimetric detection of ochratoxin A via structure-switching aptamer and enzyme-induced metallization of gold nanorods. *Food Chem.* **2020**, *320*, 126607. [[CrossRef](#)]
19. Yong, K.-T.; Sahoo, Y.; Swihart, M.T.; Prasad, P.N. Synthesis and plasmonic properties of silver and gold nanoshells on polystyrene cores of different size and of gold–silver core–shell nanostructures. *Colloids Surf. Physicochem. Eng. Asp.* **2006**, *290*, 89–105. [[CrossRef](#)]
20. Fausey, C.L.; Zucker, I.; Lee, D.E.; Shaulsky, E.; Zimmerman, J.B.; Elimelech, M. Tunable molybdenum disulfide-enabled fiber mats for high-efficiency removal of mercury from water. *ACS Appl. Mater. Interfaces* **2020**, *12*, 18446–18456. [[CrossRef](#)]
21. Wang, Z.; Mi, B. Environmental applications of 2D molybdenum disulfide (MoS₂) nanosheets. *Environ. Sci. Technol.* **2017**, *51*, 8229–8244. [[CrossRef](#)] [[PubMed](#)]
22. Wei, J.; He, P.; Wu, J.; Chen, N.; Xu, T.; Shi, E.; Pan, C.; Zhao, X.; Zhang, Y. Conversion of 2H MoS₂ to 1T MoS₂ via lithium ion doping: Effective removal of elemental mercury. *Chem. Eng. J.* **2022**, *428*, 131014. [[CrossRef](#)]
23. Zhao, H.; Yang, G.; Gao, X.; Pang, C.H.; Kingman, S.W.; Wu, T. Hg⁰ capture over CoMoS/γ-Al₂O₃ with MoS₂ nanosheets at low temperatures. *Environ. Sci. Technol.* **2016**, *50*, 1056–1064. [[CrossRef](#)] [[PubMed](#)]
24. Voiry, D.; Goswami, A.; Kappera, R.; Silva, C.d.C.C.e.; Kaplan, D.; Fujita, T.; Chen, M.; Asefa, T.; Chhowalla, M. Covalent functionalization of monolayered transition metal dichalcogenides by phase engineering. *Nat. Chem.* **2015**, *7*, 45–49. [[CrossRef](#)]
25. Wang, Z.; Sim, A.; Urban, J.J.; Mi, B. Removal and recovery of heavy metal ions by two-dimensional MoS₂ nanosheets: Performance and mechanisms. *Environ. Sci. Technol.* **2018**, *52*, 9741–9748. [[CrossRef](#)]
26. Wang, Z.; Tu, Q.; Sim, A.; Yu, J.; Duan, Y.; Poon, S.; Liu, B.; Han, Q.; Urban, J.J.; Sedlak, D.; et al. Superselective removal of lead from water by two-dimensional MoS₂ nanosheets and layer-stacked membranes. *Environ. Sci. Technol.* **2020**, *54*, 12602–12611. [[CrossRef](#)]
27. Aghagoli, M.J.; Shemirani, F. Hybrid nanosheets composed of molybdenum disulfide and reduced graphene oxide for enhanced solid phase extraction of Pb(II) and Ni(II). *Microchim. Acta* **2017**, *184*, 237–244. [[CrossRef](#)]
28. Wang, W.; Zeng, X.; Warner, J.H.; Guo, Z.; Hu, Y.; Zeng, Y.; Lu, J.; Jin, W.; Wang, S.; Lu, J.; et al. Photoresponse-bias modulation of a high-performance MoS₂ photodetector with a unique vertically stacked 2H-MoS₂/1T@2H-MoS₂ structure. *ACS Appl. Mater. Interfaces* **2020**, *12*, 33325–33335. [[CrossRef](#)]
29. Liu, B.; Han, Q.; Li, L.; Zheng, S.; Shu, Y.; Pedersen, J.A.; Wang, Z. Synergistic effect of metal cations and visible light on 2D MoS₂ nanosheet aggregation. *Environ. Sci. Technol.* **2021**, *55*, 16379–16389. [[CrossRef](#)]
30. Jia, F.; Wang, Q.; Wu, J.; Li, Y.; Song, S. Two-dimensional molybdenum disulfide as a superb adsorbent for removing Hg²⁺ from water. *ACS Sustain. Chem. Eng.* **2017**, *5*, 7410–7419. [[CrossRef](#)]
31. Urbano, F.J.; Marinas, J.M. Hydrogenolysis of organohalogen compounds over palladium supported catalysts. *J. Mol. Catal. A Chem.* **2001**, *173*, 329–345. [[CrossRef](#)]
32. Alonso, F.; Beletskaya, I.P.; Yus, M. Metal-mediated reductive hydrodehalogenation of organic halides. *Chem. Rev.* **2002**, *102*, 4009–4092. [[CrossRef](#)]
33. Ma, J.; Wei, W.; Qin, G.; Xiao, T.; Tang, W.; Zhao, S.; Jiang, L.; Liu, S. Electrochemical reduction of nitrate in a catalytic carbon membrane nano-reactor. *Water Res.* **2022**, *208*, 117862. [[CrossRef](#)]
34. Ren, Y.; Liu, Y.; Liu, F.; Li, F.; Shen, C.; Wu, Z. Extremely efficient electro-Fenton-like Sb(III) detoxification using nanoscale Ti-Ce binary oxide: An effective design to boost catalytic activity via non-radical pathway. *Chin. Chem. Lett.* **2021**, *32*, 2519–2523. [[CrossRef](#)]
35. Liu, X.Q.; Wei, W.; Xu, J.; Wang, D.B.; Song, L.; Ni, B.J. Photochemical decomposition of perfluorochemicals in contaminated water. *Water Res.* **2020**, *186*, 116311. [[CrossRef](#)]
36. Liu, F.; Liu, Y.; Yao, Q.; Wang, Y.; Fang, X.; Shen, C.; Li, F.; Huang, M.; Wang, Z.; Sand, W.; et al. Supported atomically-precise gold nanoclusters for enhanced flow-through electro-Fenton. *Environ. Sci. Technol.* **2020**, *54*, 5913–5921. [[CrossRef](#)]
37. Li, Z.M.; Zhang, P.Y.; Shao, T.; Wang, J.L.; Jin, L.; Li, X.Y. Different nanostructured In₂O₃ for photocatalytic decomposition of perfluorooctanoic acid (PFOA). *J. Hazard. Mater.* **2013**, *260*, 40–46. [[CrossRef](#)]
38. Liu, F.; You, S.; Wang, Z.; Liu, Y. Redox-active nanohybrid filter for selective recovery of gold from water. *ACS EST Eng.* **2021**, *1*, 1342–1350. [[CrossRef](#)]
39. Zhong, Y.; Li, T.; Lin, H.; Zhang, L.; Xiong, Z.; Fang, Q.; Zhang, G.; Liu, F. Meso-/macro-porous microspheres confining Au nanoparticles based on PDLA/PLLA stereo-complex membrane for continuous flowing catalysis and separation. *Chem. Eng. J.* **2018**, *344*, 299–310. [[CrossRef](#)]
40. Liu, Y.; Zheng, Y.; Du, B.; Nasaruddin, R.R.; Chen, T.; Xie, J. Golden carbon nanotube membrane for continuous flow catalysis. *Ind. Eng. Chem. Res.* **2017**, *56*, 2999–3007. [[CrossRef](#)]
41. Wu, C.; Zhu, X.; Wang, Z.; Yang, J.; Li, Y.; Gu, J. Specific recovery and in situ reduction of precious metals from waste to create MOF composites with immobilized nanoclusters. *Ind. Eng. Chem. Res.* **2017**, *56*, 13975–13982. [[CrossRef](#)]
42. Zheng, W.; Liu, Y.; Liu, W.; Ji, H.; Li, F.; Shen, C.; Fang, X.; Li, X.; Duan, X. A novel electrocatalytic filtration system with carbon nanotube supported nanoscale zerovalent copper toward ultrafast oxidation of organic pollutants. *Water Res.* **2021**, *194*, 116961. [[CrossRef](#)] [[PubMed](#)]

43. Zhang, Q.; Li, M.; Luo, B.; Luo, Y.; Jiang, H.; Chen, C.; Wang, S.; Min, D. In situ growth gold nanoparticles in three-dimensional sugarcane membrane for flow catalytical and antibacterial application. *J. Hazard. Mater.* **2021**, *402*, 123445. [[CrossRef](#)]
44. Liang, M.; Su, R.; Huang, R.; Qi, W.; Yu, Y.; Wang, L.; He, Z. Facile in situ synthesis of silver nanoparticles on procyanidin-grafted eggshell membrane and their catalytic properties. *ACS Appl. Mater. Interfaces* **2014**, *6*, 4638–4649. [[CrossRef](#)] [[PubMed](#)]
45. Liu, F.; Liu, Y.; Shen, C.; Li, F.; Yang, B.; Huang, M.; Ma, C.; Yang, M.; Wang, Z.; Sand, W. One-step phosphite removal by an electroactive CNT filter functionalized with TiO₂/CeO_x nanocomposites. *Sci. Total Environ.* **2020**, *710*, 135514. [[CrossRef](#)] [[PubMed](#)]
46. Mao, R.; Zhao, X.; Qu, J. Electrochemical reduction of bromate by a Pd modified carbon fiber rlectrode: Kinetics and mechanism. *Electrochim. Acta* **2014**, *132*, 151–157. [[CrossRef](#)]
47. Gao, P.; Martin, C.R. Voltage charging rhnances ionic conductivity in gold nanotube membranes. *ACS Nano* **2014**, *8*, 8266–8272. [[CrossRef](#)] [[PubMed](#)]
48. Soares, O.S.G.P.; Ramalho, P.S.F.; Fernandes, A.; Órfão, J.J.M.; Pereira, M.F.R. Catalytic bromate reduction in water: Influence of carbon support. *J. Environ. Chem. Eng.* **2019**, *7*, 103015. [[CrossRef](#)]
49. Wang, J.; Wu, C.; Hu, N.; Zhou, J.; Du, L.; Wang, P. Microfabricated electrochemical cell-based biosensors for analysis of living cells in vitro. *Biosensors* **2012**, *2*, 127. [[CrossRef](#)]
50. Zhang, Y.; Sun, J.; Hou, B.; Hu, Y. Performance improvement of air-cathode single-chamber microbial fuel cell using a mesoporous carbon modified anode. *J. Power Sources* **2011**, *196*, 7458–7464. [[CrossRef](#)]
51. Perez-Coronado, A.M.; Soares, O.S.G.P.; Calvo, L.; Rodriguez, J.J.; Gilarranz, M.A.; Pereira, M.F.R. Catalytic reduction of bromate over catalysts based on Pd nanoparticles synthesized via water-in-oil microemulsion. *Appl. Catal. B* **2018**, *237*, 206–213. [[CrossRef](#)]
52. Yao, F.; Yang, Q.; Yan, M.; Li, X.; Chen, F.; Zhong, Y.; Yin, H.; Chen, S.; Fu, J.; Wang, D.; et al. Synergistic adsorption and electrocatalytic reduction of bromate by Pd/N-doped loofah sponge-derived biochar electrode. *J. Hazard. Mater.* **2020**, *386*, 121651. [[CrossRef](#)]
53. Madhushree, R.; UC, J.R.J.; Pinheiro, D.; KR, S.D. The catalytic reduction of 4-nitrophenol using MoS₂/ZnO nanocomposite. *Appl. Surf. Sci. Adv.* **2022**, *10*, 100265. [[CrossRef](#)]
54. Zhang, Z.-M.; Cheng, R.; Nan, J.; Chen, X.-Q.; Huang, C.; Cao, D.; Bai, C.-H.; Han, J.-L.; Liang, B.; Li, Z.-L.; et al. Effective electrocatalytic hydrodechlorination of 2,4,6-trichlorophenol by a novel Pd/MnO₂/Ni foam cathode. *Chin. Chem. Lett.* **2022**, *33*, 3823–3828. [[CrossRef](#)]
55. Kishimoto, N.; Matsuda, N. Bromate ion removal by electrochemical reduction using an activated carbon felt electrode. *Environ. Sci. Technol.* **2009**, *43*, 2054–2059. [[CrossRef](#)]
56. Koga, H.; Namba, N.; Takahashi, T.; Nogi, M.; Nishina, Y. Renewable wood pulp paper reactor with hierarchical micro/nanopores for continuous-flow nanocatalysis. *Chem. Sus. Chem* **2017**, *10*, 2560–2565. [[CrossRef](#)]
57. Gopiraman, M.; Saravanamoorthy, S.; Baskar, R.; Ilangovan, A.; Ill-Min, C. Green synthesis of Ag@Au bimetallic regenerated cellulose nanofibers for catalytic applications. *New J. Chem.* **2019**, *43*, 17090–17103. [[CrossRef](#)]
58. Yu, X.-F.; Mao, L.-B.; Ge, J.; Yu, Z.-L.; Liu, J.-W.; Yu, S.-H. Three-dimensional melamine sponge loaded with Au/ceria nanowires for continuous reduction of p-nitrophenol in a consecutive flow system. *Sci. Bull.* **2016**, *61*, 700–705. [[CrossRef](#)]
59. Massaro, M.; Colletti, C.G.; Fiore, B.; La Parola, V.; Lazzara, G.; Guernelli, S.; Zaccheroni, N.; Riela, S. Gold nanoparticles stabilized by modified halloysite nanotubes for catalytic applications. *Appl. Organomet. Chem.* **2019**, *33*, e4665. [[CrossRef](#)]
60. Liu, X.; Li, Y.; Xing, Z.; Zhao, X.; Liu, N.; Chen, F. Monolithic carbon foam-supported Au nanoparticles with excellent catalytic performance in a fixed-bed system. *New J. Chem.* **2017**, *41*, 15027–15032. [[CrossRef](#)]